Volume 61
Number 96
14 December 2025
Pages 18925–19134

ChemComm

Chemical Communications

rsc.li/chemcomm

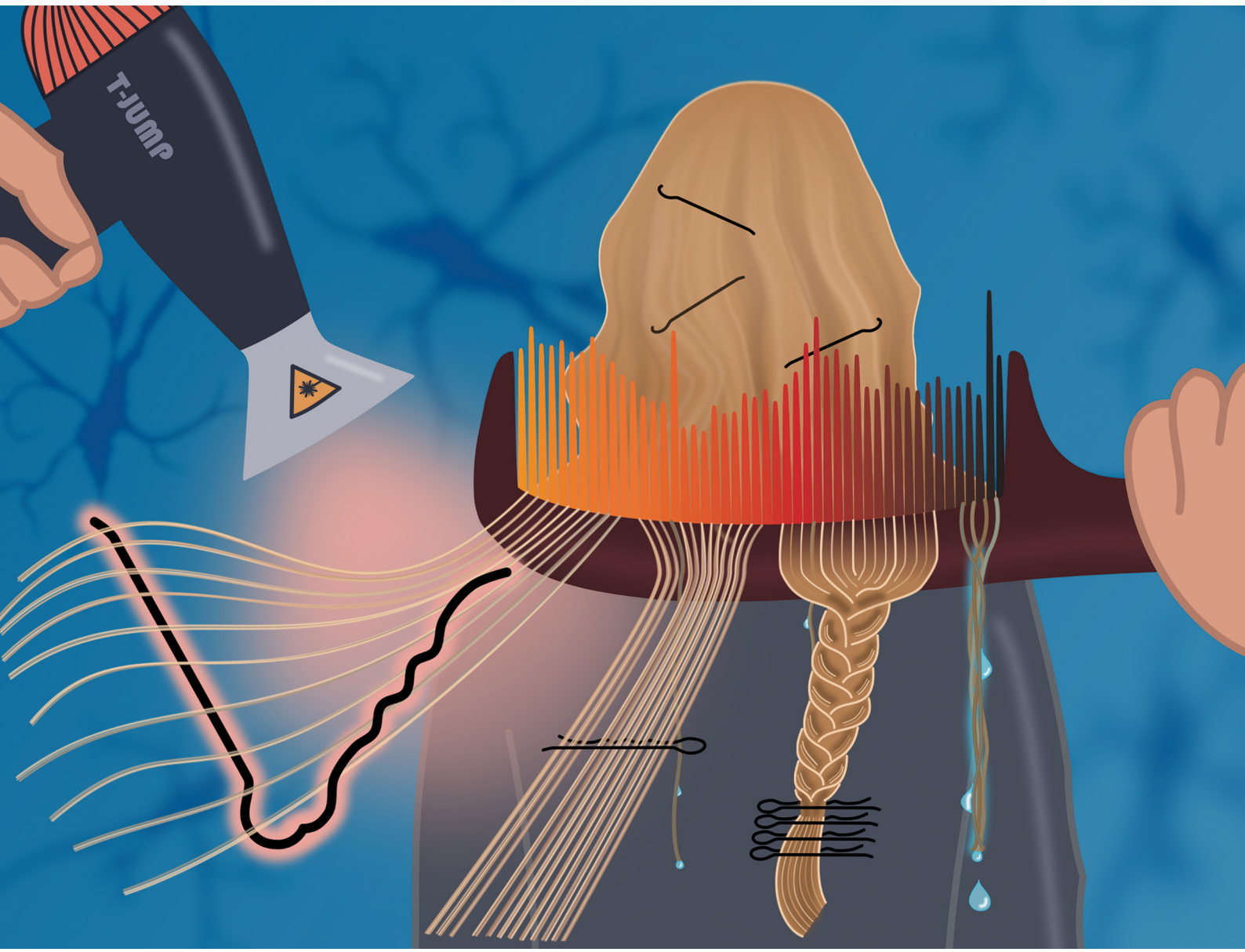

ISSN 1359-7345

ROYAL SOCIETY OF CHEMISTRY

COMMUNICATION

Lorenz Mattes, Paul Stritt, Karin Hauser *et al.*
Temperature-jump QCL spectroscopy of peptide dynamics: expanding spectral accessibility by dual-combs

ChemComm

COMMUNICATION

View Article Online
View Journal | View Issue

Cite this: *Chem. Commun.*, 2025, **61**, 19024

Received 12th August 2025,
Accepted 9th October 2025

DOI: 10.1039/d5cc04629g

rsc.li/chemcomm

Temperature-jump QCL spectroscopy of peptide dynamics: expanding spectral accessibility by dual-combs

Lorenz Mattes, [a] Manuel Oestringer, [a] Paul Stritt, [a] Raphael Horvath, [b] Andreas Hugi [b] and Karin Hauser *[a]

Combining infrared dual-comb spectroscopy with laser-induced nanosecond temperature-jumps enables fast tracking of peptide folding dynamics. Compared to single-wavenumber quantum cascade lasers, this method provides broader spectral information. Using a model peptide system, the study opens new perspectives for applying time-resolved IR spectroscopy to explore mechanistic details in biomolecular dynamics.

Time-resolved infrared (IR) spectroscopy is a powerful technique for studying peptide folding dynamics, as it captures structural changes through the amide I band. Traditional Fourier-transform infrared (FTIR) spectroscopy, when combined with perturbation methods such as temperature-jump (T-jump), allows real-time observation of folding kinetics. Rapid-scan FTIR offers millisecond time resolution *via* continuous acquisition, while step-scan FTIR reaches micro- and even nanosecond resolution by recording interferograms stepwise. A key advantage of FTIR methods is their broadband spectral coverage, enabling simultaneous observation across multiple vibrational modes. However, their reliance on thermal light sources like globars limits intensity, often requiring extensive averaging to achieve a sufficient signal-to-noise ratio.

Single-wavenumber quantum cascade laser (SW-QCL) spectroscopy addresses these limitations by providing high-intensity, tunable mid-IR light at selected wavenumbers. In T-jump experiments, SW-QCLs have enabled the observation of fast folding processes with excellent signal-to-noise ratio and data quality. However, their narrow spectral bandwidth restricts the ability to capture transient structural intermediates across the full amide I region, and tuning across wavenumbers requires multiple measurements.[1–6]

A major advance in mid-IR spectroscopy is the development of QCL-based frequency combs. Dual-comb spectroscopy (DCS) offers a unique combination of broadband spectral coverage ($\sim$70 cm^{-1} comb bandwidth in this study), high brightness, and precise frequency referencing.[7–9] This enables rapid, multiplexed acquisition of vibrational spectra with high temporal resolution – well suited for studying fast, non-repetitive processes. DCS has been applied to time-resolved studies such as photoreactions of bacteriorhodopsin,[10,11] caged compounds[12] and irreversible photoreactions of visual rhodopsin,[13] but has not yet been explored in T-jump peptide folding experiments.

Here, we present a comparative study of IR DCS and SW-QCL spectroscopy for nanosecond T-jump experiments. As a model system, we investigate the folding dynamics of the glutamine-containing peptide Trpzip-Q_2 (SWQWENGKWQWK-NH_2), which adopts a β-hairpin structure. β-Hairpins are thought to act as critical intermediates in polyglutamine (polyQ) aggregation, a process implicated in neurodegenerative disorders such as Huntington's disease.[14,15] PolyQ tracts beyond a pathological threshold of 35–40 residues tend to misfold and form amyloid-like fibrils.[16,17] Hydrogen bonding between glutamine side chains and peptide backbones is believed to drive this aggregation, stabilizing β-sheet-rich structures. Short peptide models such as Trpzip-Q_2 allow a detailed and tractable investigation of early structural transitions that may nucleate these aggregation pathways. Moreover, their accessibility to isotope labelling makes them ideal systems for residue-specific folding studies.[3,4]

T-jump experiments with SW-QCLs have provided detailed insights into peptide folding dynamics, including polyQ-rich β-hairpin models.[18,19] By applying both DCS and SW-QCL spectroscopy to the model peptide Trpzip-Q_2, we establish a benchmark for evaluating the capabilities and limitations of each method. Beyond validating a new spectroscopic approach, this work opens a new perspective for future applications of DCS in tracking sub-millisecond folding and misfolding dynamics in peptide and protein systems.

To experimentally evaluate both DCS and SW-QCL spectroscopy under identical conditions, we measured Trpzip-Q_2 dissolved in D_2O using a CaF_2 transmission cuvette. Our setup

[a] *Department of Chemistry, University of Konstanz, 78457 Konstanz, Germany. E-mail: karin.hauser@uni-konstanz.de*
[b] *Sensirion AG, 8712 Stäfa, Switzerland*

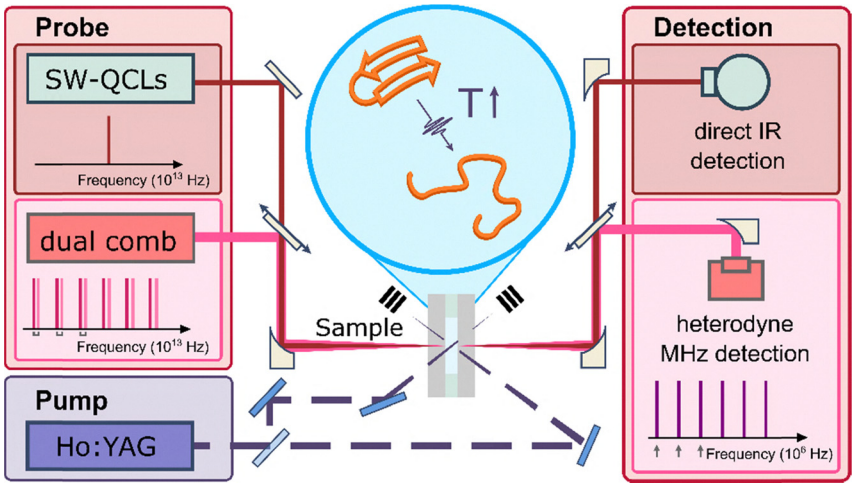

Fig. 1 Sketch of the laser spectroscopy setup to monitor unfolding dynamics of β-hairpin peptides after a laser-induced temperature-jump by a pulsed Ho:YAG laser. The absorbance change can be measured either with single-wavenumber QCL or QCL-based dual-comb spectroscopy.

allows for seamless switching between the two spectroscopic techniques by simply inserting mirrors to select the desired beam path through the sample. To probe fast dynamic processes, a nanosecond-scale T-jump of about 21 K was induced using a pulsed Ho:YAG laser (IPG Photonics, USA) to excite an overtone vibration of the solvent. The magnitude of the T-jump was determined from the characteristic absorbance change of D_2O. A sketch of the experimental setup, including both spectroscopic beam pathways and the T-jump configuration, is shown in Fig. 1. A detailed schematic diagram of the home-built laser setup is shown in Fig. S1 in the SI.

The peptide response following the T-jump was measured with both continuous-wave QCL-based infrared spectroscopic methods:

For SW-QCL spectroscopy, a MIRcat-QT system (DRS Daylight Solutions, USA) was used. The QCL had a tuning range of 1475–1750 cm^{-1} with a step size of 0.5 cm^{-1}, and measurements were conducted at selected wavenumbers (1630, 1632, 1657 and 1659 cm^{-1}). Detection was performed using a liquid nitrogen-cooled mercury cadmium telluride (MCT) detector with a rise time of 20 ns, and data were recorded at a sampling rate of 105 MS s^{-1}. Each transient was averaged over 1000 single measurements. For dual-comb spectroscopy (DCS), an IRis-F1 spectrometer (Thorlabs, USA; formerly IRsweep, Switzerland) was used, providing spectral coverage of 1589–1659 cm^{-1} with approximately 220 comb teeth. Time-resolved spectra were recorded at 1 μs resolution, averaging over 100 000 measurements.

To isolate the peptide signal from the strong D_2O background (∼10× larger), reference transients of pure D_2O were recorded. These were scaled to the late-time region of the sample transient, where the peptide dynamics were no longer evolving, to ensure optimal subtraction. Logarithmic averaging was applied to get the same number of data points in each decade, and peptide relaxation kinetics were extracted by monoexponential fitting from 200 ns (for SW-QCL) and 1 μs (for DCS) to 200 μs. Further details are provided in the SI.

A direct comparison of transient absorbance changes measured with both techniques is shown in Fig. 2. The wavenumbers selected for analysis – 1632 and 1659 cm^{-1} – correspond to the most intense spectral changes in the amide I' band, which can also be observed in temperature-dependent equilibrium FTIR spectra (Fig. S2). Both data sets reflect the decline of β-sheet structure and the rise of disordered structure after the T-jump. On a first visual inspection, the transients from both techniques appear similar, and the absolute absorbance changes are in the same range of approximately 1 to 1.5 mOD.

Examining the early time points highlights key differences in measurement quality. The two techniques differ notably in their time resolution. The SW-QCL method provides significantly more data points in the initial phase of the transient, allowing better resolution of fast kinetics. In contrast, the DCS data start at 1 μs, and due to the inherent 1 μs time resolution, the initial part of the transient remains relatively noisy, as the logarithmic averaging does not sufficiently smooth out fluctuations at shorter timescales. The time resolution could be improved by reducing the Fast Fourier Transform (FFT) length. However, this would lead to a deterioration in the signal-to-noise ratio. As the transient progresses, the noise level decreases due to logarithmic averaging, making the later stages of the decay more reliable. Moreover, the full spectral data set provided by DCS lends itself to global fitting, which can improve the robustness of extracted kinetics compared to independent single-wavenumber fits. In the present case, however, the proximity of the time constants limited the ability of global analysis to separate them.

A more general noise comparison further illustrates the strengths and limitations of each technique. The SW-QCL provides a higher signal-to-noise ratio due to its higher light intensity per wavenumber. In contrast, the DCS method distributes intensity across many comb teeth, leading to substantially lower intensity per wavenumber. The noise level also varies significantly between different comb teeth, as some wavenumbers are strongly affected by water vapor absorption in the setup. Despite purging with dried air, minor residual

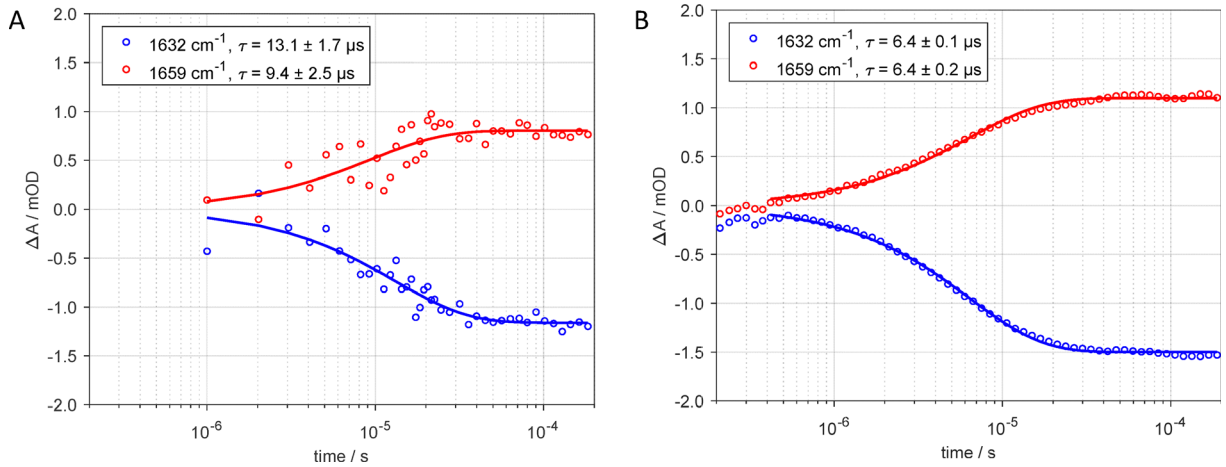

Fig. 2 Transients at single wavenumbers showing most significant changes in temperature-jump measurements of Trpzip-Q_2 with (A) dual-comb spectroscopy and (B) SW-QCL spectroscopy. 1632 cm^{-1} shows the loss of β-structure, whereas 1659 cm^{-1} shows the rise of disordered structure. Whereas the time resolution and signal-to-noise ratio of the SW-QCL clearly exceeds the dual-comb, monoexponential fits of the transients of both techniques show a good consensus in time constants.

humidity absorption reduces the intensity of certain comb teeth, particularly in spectral regions overlapping with water vapor absorption bands. Additionally, low-intensity comb teeth at the spectral edges further contribute to variable noise levels.

The extracted time constants from monoexponential fits highlight additional differences between the techniques. For SW-QCL, the β-hairpin loss at 1632 cm^{-1} and the rise of disordered structure at 1659 cm^{-1} show identical time constants of 6.4 µs. In contrast, the DCS results show greater variability: time constants of 13.1 µs at 1632 cm^{-1} and 9.4 µs at 1659 cm^{-1}. Additional data and fit results are presented in the SI Fig. S4, Table S1 and Fig. S5. This variation suggests that the DCS method provides less uniform results, likely due to the limited time resolution and greater noise levels. Despite this, the general trend of β-sheet loss occurring slightly slower than the rise of disordered structure remains consistent across both techniques.

Overall, these observations demonstrate the trade-offs between the two methods: SW-QCL offers superior time resolution and lower noise, whereas DCS provides broader spectral coverage, albeit with higher noise and slightly reduced reliability in kinetic parameter extraction. The full DCS data set (Fig. 3 and Fig. S3) provides a comprehensive view of the spectral evolution, clearly showing the overall changes within the amide I' band, with β-sheet loss around 1632 cm^{-1} and the rise of disordered structure near 1660 cm^{-1}. However, the data

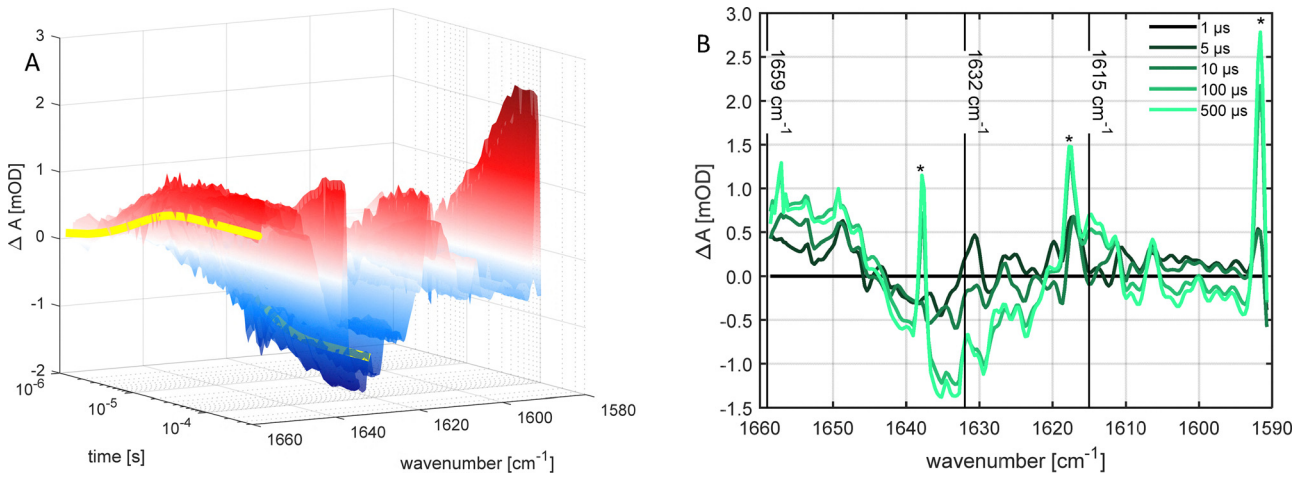

Fig. 3 (A) Full spectral view of the peptide folding dynamics recorded with the dual-comb laser spectrometer. Following T-jump excitation, the absorbance changes reveal a loss of β-hairpin structure and a rise of disordered conformations in the amide I' region of Trpzip-Q_2. The dual-comb spectrometer provides coverage of approximately 70 cm^{-1} with 1 µs time resolution. In the 3D plot, the transients shown in Fig. 2 are highlighted in yellow. (B) Difference spectra at selected time slices, derived from logarithmically averaged data. While logarithmic averaging reduces the apparent scattering of the data, subtraction of the first spectrum introduces its temporal fluctuations into all subsequent difference spectra. Water vapor and low comb intensities can cause artifacts marked with asterisks. The band at 1615 cm^{-1} is highlighted, where its increasing absorbance suggests the formation of oligomers in the sample.

set also highlights gaps in spectral coverage where individual comb teeth exhibit high noise or unreliable transients due to moisture absorption, limiting the interpretability of certain spectral regions. Additionally, the spectral range of the comb setup ends at 1660 cm^{-1}, meaning the full extent of the rise in disordered structure is not entirely captured.

Importantly, the broad spectral access of the DCS method also reveals a previously overlooked feature: an emerging absorbance around 1615 cm^{-1}, visible in Fig. 3. This subtle but distinct signal was not evident in SW-QCL measurements due to its focus on selected wavenumbers. Its presence suggests early-stage oligomer formation in the sample,[20–22] which was not apparent from visual inspection of sample transparency. Initial aggregation processes may have been triggered by cooling and could be captured only through the broadband capability of the dual-comb approach. This finding underscores the added value of DCS broad spectral coverage in identifying unexpected structural intermediates during folding kinetics.

In summary, our findings underline the complementary nature of both techniques in studying peptide folding dynamics. While SW-QCL spectroscopy excels in capturing fast kinetics with high signal-to-noise ratio, DCS provides extensive spectral information that enables a more comprehensive view of structural evolution. The applicability of each technique depends strongly on the timescale of the studied process. The DCS setup used here performs well for slower systems, but for faster kinetics as observed in this study, it approaches the limit of accurate analysis. Further refinements, such as increased detection sensitivity and improved spectral intensity distribution, could enhance its capability to study even faster systems.

One major perspective of the DCS approach is its suitability for isotope-labeling experiments, which allow for residue-specific insights into peptide folding kinetics and stability.[3,4] By recording an entire spectral window simultaneously, DCS can capture the often-unknown positions of isotope-shifted amide I bands. In addition, both wavenumber shifts and population changes can be resolved, which is challenging with single-frequency approaches as they require pre-selecting of probe wavenumbers. This capability enables a deeper understanding of individual amino-acid contributions to folding mechanisms. This step forward in methodology has significant implications for protein folding and misfolding studies, particularly in disease-related contexts.

Ultimately, the choice between these methods depends on the specific research question. For kinetic precision, SW-QCL is preferable, while for broader spectral insights and isotope-labeling applications, DCS holds great promise. The straightforward switching between the techniques *via* flip-mounted mirrors further enhances their practicality, making them highly adaptable tools for advancing the field of protein folding research by time-resolved IR spectroscopy.

This work was supported by the Deutsche Forschungsgemeinschaft (DFG, German Research Foundation, grant numbers: CRC 969, A2 and 564132680).

LM: data curation; formal analysis; investigation; writing – original draft; software. MO: formal analysis; investigation; software. PS: investigation; methodology. RH: methodology; software. AH: methodology. KH: conceptualization; funding acquisition; writing – review & editing; supervision.

Conflicts of interest

There are no conflicts to declare.

Data availability

The data supporting this article (schematic diagram of setup, sample preparation, measurement conditions, data analysis, FTIR equilibrium measurements, additional fit results) have been included as part of the supplementary information (SI). Supplementary information is available. See DOI: **https://doi.org/10.1039/d5cc04629g**.

References

1 C. M. Davis and R. B. Dyer, *J. Am. Chem. Soc.*, 2013, **135**, 19260–19267.
2 P. Stritt, M. Jawurek and K. Hauser, *Biomed. Spectrosc. Imaging*, 2020, **9**, 55–61.
3 D. Scheerer, H. Chi, D. McElheny, T. A. Keiderling and K. Hauser, *J. Phys. Chem. B*, 2018, **122**, 10445–10454.
4 D. Scheerer, H. Chi, D. McElheny, T. A. Keiderling and K. Hauser, *Chemistry*, 2020, **26**, 3524–3534.
5 B. J. Schultz, H. Mohrmann, V. A. Lorenz-Fonfria and J. Heberle, *Spectrochim. Acta, Part A*, 2018, **188**, 666–674.
6 P. Stritt, M. Jawurek and K. Hauser, *J. Chem. Phys.*, 2023, **158**, 154202.
7 J. Hayden, M. Geiser, M. Gianella, R. Horvath, A. Hugi, L. Sterczewski and M. Mangold, *APL Photonics*, 2024, **9**, 031101.
8 A. Hugi, G. Villares, S. Blaser, H. C. Liu and J. Faist, *Nature*, 2012, **492**, 229–233.
9 G. Villares, A. Hugi, S. Blaser and J. Faist, *Nat. Commun.*, 2014, **5**, 5192.
10 L. Schubert, P. Langner, D. Ehrenberg, V. A. Lorenz-Fonfria and J. Heberle, *J. Chem. Phys.*, 2022, **156**, 204201.
11 J. L. Klocke, M. Mangold, P. Allmendinger, A. Hugi, M. Geiser, P. Jouy, J. Faist and T. Kottke, *Anal. Chem.*, 2018, **90**, 10494–10500.
12 M. J. Norahan, R. Horvath, N. Woitzik, P. Jouy, F. Eigenmann, K. Gerwert and C. Kötting, *Anal. Chem.*, 2021, **93**, 6779–6783.
13 L. Schubert, F. Bartl and J. Heberle, *Biophys. J.*, 2025, **124**, DOI: **10.1016/j.bpj.2025.06.030**.
14 S. W. Davies, M. Turmaine, B. A. Cozens, M. DiFiglia, A. H. Sharp, C. A. Ross, E. Scherzinger, E. E. Wanker, L. Mangiarini and G. P. Bates, *Cell*, 1997, **90**, 537–548.
15 M. DiFiglia, E. Sapp, K. O. Chase, S. W. Davies, G. P. Bates, J. P. Vonsattel and N. Aronin, *Science*, 1997, **277**, 1990–1993.
16 S. Chen, F. A. Ferrone and R. Wetzel, *Proc. Natl. Acad. Sci. U. S. A.*, 2002, **99**, 11884–11889.
17 K. Kar, M. Jayaraman, B. Sahoo, R. Kodali and R. Wetzel, *Nat. Struct. Mol. Biol.*, 2011, **18**, 328.
18 H.-W. Siu and K. Hauser, *J. Phys. Chem. Lett.*, 2022, **13**, 4543–4548.
19 H.-W. Siu, B. Heck, M. Kovermann and K. Hauser, *Chem. Sci.*, 2021, **12**, 412–426.
20 B. S. Heck, F. Doll and K. Hauser, *Biophys. Chem.*, 2014, **185**, 47–57.
21 J. P. Lomont, J. S. Ostrander, J. J. Ho, M. K. Petti and M. T. Zanni, *J. Phys. Chem. B*, 2017, **121**, 8935–8945.
22 S. D. Moran and M. T. Zanni, *J. Phys. Chem. Lett.*, 2014, **5**, 1984–1993.